An engineering model for rapid crack propagation along fluid pressurised plastic pipe

Patrick Leevers

Mechanical Engineering Department, Imperial College London
London SW7 2AZ, UK

Abstract

The appearance of new materials has revived interest in the modelling of rapid crack propagation (RCP) along fluid-pressurised plastic pipelines. The correlation of results from two International Standard RCP test methods — one full-scale and partially simulating installation and service conditions, the other lab-scale — remains imperfectly understood. There is no standard method for measuring the dynamic fracture toughness of the pipe material, and models relating toughness to pipe fracture pressure have not gained widespread use. This paper demonstrates an adaptable, extendable, analytically transparent model which accounts for all major influences including residual stress in the pipe wall, constraint from surrounding backfill and partial substitution of the pressurising gas by water.

Keywords: Polymers, Fracture mechanics, Dynamic fracture, Pipelines, Failure assessment

1. Introduction

Because rapid crack propagation (RCP) failures in plastic pipe are so rare, the régime of standards and test methods which made them so has begun to seem oppressive. The understanding of RCP built up over 25 years of research has been challenged by new materials, processes and observations during the decade since basic research was cut back. This is partly because researchers had not delivered a single, commonly accepted model, sufficiently accessible for users to adopt and develop. The present paper addresses that issue and demonstrates a solution.

RCP along a pipeline is characterised by steady axial crack propagation, at a speed comparable to that of decompression in the pressurising fluid, above a *critical pressure* — below which there is prompt crack arrest. It was first identified as a distinct problem in steel linepipe for gas transmission. As recounted by Leis [1], the role of fracture mechanics in research to avoid RCP

Email address: p.leevers@imperial.ac.uk (Patrick Leevers)

changed as steels overtook, and were again overtaken by the operating pressure demands made on them. Thermoplastics suitable for pipe extrusion, however, have a yield strain high enough, and a mode of high-speed crack propagation brittle enough, for LEFM to suffice at the pressures of interest. Early experiments by Shannon and Wells [2] on PVC were developed by Greig [3] into the Full Scale test method, later to become international standard ISO 13478, for the tougher polyethylene (PE) materials. Subsequent generations of PE now dominate low-pressure gas and water distribution pipe networks.

The classical, quasi-static LEFM analysis of Irwin and Corten [4] led to a closed-form expression for crack driving force:

$$G \equiv G_0 = \frac{\pi p_0^2 \left(D-2h\right)^2 \left(D-h\right)}{8Eh^2} = \frac{\pi}{8}\frac{p_0^2}{E_\mathrm{d}} D \frac{\left(D^*-2\right)^2 \left(D^*-1\right)}{D^*} \qquad (1)$$

where p_0 is the initial line gauge pressure, D and h are the outside diameter and wall thickness of the pipe, D^* is their ratio D/h and E_d is the tensile modulus of the material at an appropriate time scale. Equating Eq. (1) to the dynamic fracture resistance G_d of the pipe wall material predicts a critical pressure:

$$p_{\mathrm{c}0} = \frac{1}{\left(D^*-2\right)} \sqrt{\frac{8}{\pi}\frac{E_\mathrm{d} G_\mathrm{d}}{D}\frac{D^*}{\left(D^*-1\right)}}. \qquad (2)$$

The appealingly simple 'Irwin-Corten equation' (2) seemed at first to explain full-scale test results using toughness data from sharp-notched Charpy test data. As linepipe steels improved, however, RCP was driven into the ductile régime. Here, large deformations and significant kinetic energy exchanges demand the use of dynamic fracture mechanics and a steady-state, propagation-mode analysis (Fig. 1). The crack driving force $G(\dot{a})$ is calculated, and dynamic fracture resistance $G_\mathrm{d}(\dot{a})$ is measured, as a function of constant crack speed $\dot{a}$. Developed during the 1970s by Kanninen and colleagues at Batelle's Columbus laboratories, this approach still dominates the problem. Elastic-plastic shell analysis was applied to analyse steel linepipe without [5] and later with backfill [6]. In each case the outcome was a fourth-order differential equation for the variation of crack opening w with distance z behind the crack front. Solutions $w(z)$ led directly to the time derivatives of strain energy, kinetic energy and pressure work terms and hence to the crack-driving force G which balances them.

Kanninen, and co-workers O'Donoghue [7], re-formulated the dynamic model for finite-element solution and applied it to plastic pipe. For these lower strength materials the dynamic influences on G — fluid outflow through the crack, backflow from the pipe ahead, inertia of the pipe wall and (if present) backfill — assume even greater importance. Semi-crystalline polymers are also much more rate-sensitive than steel in their elastic [8], plastic [9] and impact fracture [10] properties. There is no established test method for measuring $G_\mathrm{d}(\dot{a})$ at $\dot{a}$ =100–300 m/s. Figure 1 is sketched from the few available data, a single material model [10] and general observations of polymer fracture dynamics: for tough thermoplastics G_d depends strongly on crack speed $\dot{a}$ as well as on temperature

and wall thickness. Note that $G(\dot{a})$ curves computed for pipe fully or partially pressurised by gas share this bell shape, with a peak value typically many times greater than G_0[11]. Where $p > p_c$ and $G(\dot{a})$ intersects $G_d(\dot{a})$ twice, only the right-hand point can be observed as a stable state.

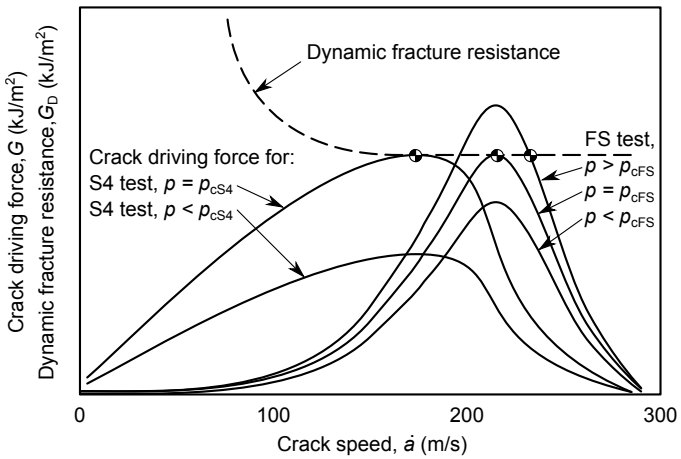


Figure 1: Schematic showing the dependence of crack driving force (solid lines) and crack resistance on crack speed in pressurised PE pipe. The intersection points shown represent stable RCP.

In Europe, some large-scale RCP failures during proof testing of PE systems hastened the search for a small-scale test method robust enough to underpin international pipe product specifications. The S4 (Small Scale Steady State) test, developed [12] as an RCP research tool, was adopted as an International Standard (ISO 13477) pipe test and remains widely used for material development.

1.1. Problem issues for RCP testing

Critical pressures p_{cS4} measured in the S4 test are much lower than those from the more realistic FS test, p_{cFS}. Wölters [13] explained this (as Maxey [14] had for steel pipe) using a model based on axial backflow dynamics of the pressurising gas and independent of the pipe material. The correlation factor written into ISO 13477,

$$p_{cFS} = 3.6 p_{cS4} + 2.6 \text{ (bar)}, \tag{3}$$

is based on this model and on the questionable assumption that the crack arrests by quasi-static deceleration. In PE at least, that does not happen: stable RCP has not been observed at less than 100-150 m/s [15, 16, 17], for which the decompression ratio is much less than the predicted static value 3.6. Yet p_{cFS}/p_{cS4} data support 3.6 as a lower bound [18] rather than an upper bound. Worse, recent results from tests on polyamide pipe [19] appear systematically to support a much higher correlation factor, and advocates of this material allege

over-conservatism. Kanninen [20] and Grigory [21] pointed out that *if* G_{d} did not depend strongly on crack speed and $G(\dot{a})$ curves for the S4 and full scale (FS) tests could be determined, a full-scale critical pressure could be predicted from an S4 critical pressure result, as implied in Fig. 1. The S4 test would then revert to its origin as a material test, and the FS-S4 'correlation factor' $p_{\mathrm{cFS}}/p_{\mathrm{cS4}}$ would be determined *ad hoc*. For the moment, however, Eq. (3) stands by default.

Meanwhile, S4 tests at high pressures sometimes show 'false arrests' of RCP. The method was adjusted in ISO13477:2007 to discourage its use at pressures which are in any case unrepresentative of service conditions. The problem was thereby suppressed rather than understood.

Another potential influence on $p_{\mathrm{cFS}}/p_{\mathrm{cS4}}$ correlation is backfill, which is required in the FS method but absent in the S4 method. The role of backfill was recognised long ago for steel pipe and studied more recently in this context both computationally using finite element analysis [22] and experimentally using the S4 test [23]. Grigory [21] argued that "... the partially buried condition of the test pipe in the [FS] test is a flaw that prevents the data from being used to predict the critical pressure for any operating condition". This would no longer be the case if the backfill effect were understood and could be factored out.

It will be argued here that the influence of backfill is closely related to that of partially replacing the pressurising air by water. Service RCP incidents in water pipelines are rare but they do occur [24], and research has provided information which is yet to be fully integrated with our understanding of RCP in gas-pressurised pipe [25].

Finally, there are unanswered questions on the effect of residual strain. Greenshields [26] argued that the strain distribution (compressive on the outside surface, tensile on the inner surface) normally frozen into pipe by post-extrusion external cooling, must be overcome by an additional internal pressure, so increasing the RCP critical pressure. Qualitiative support came from FS tests on pipe made using dual-surface cooling [23], which balances the residual strain field and eliminates the closure moment but also damages RCP performance. On the other hand, residual stress alone has been known to drive a crack, and Lamborn [27] achieved significantly improved PE pipe S4 results by annealing it out.

1.2. The case for an open RCP model

This long list of issues confuses and frustrates the developers of new pipe-grade polymers and pipe production processes. Even the 'small-scale' S4 RCP test is too expensive for them; they need a tool for *virtual* testing, transparently based on a common understanding of RCP mechanisms. At least two such tools have already been developed, both embodied in large and complicated computer codes: O'Donoghue, Kanninen *et al.* [7, 28] and Zhuang [29, 22, 30, 31] used a coupled shell finite element and fluid finite volume method, Ivankovic [32] and successive co-workers [33] an integrated finite volume one. Users understandably treat large, specialised, non-commercial software warily [21] and neither code gained general use. In the complexity of the problem and of its discretisation,

it is too easy to lose sight of the physical principles; this makes it difficult to verify results, and undermines their credibility.

Analytical methods are more transparent but have not been more successful. The Irwin-Corten analysis [4] is strictly applicable only to a pipe pressurised by an internal solid (like the district heating casing pipe in which RCP was studied by Nilsson [34]) or, under special conditions, by water [35], but not by gas. The beam-bending models of Williams [36], and of Kanninen [37] before him, inspired the present one, but then evolved towards daunting complexity. The model presented here is implemented in an accessible, modular C++ library and is open for development as the understanding of RCP advances. The only numerical method it uses is a standard finite difference method which could, in principle, be implemented in a spreadsheet.

2. The RCP model

Figure 2 represents a crack propagating steadily along a pipeline whose initial internal fluid pressure was p_0. The pressure is $p_1 \leq p_0$ at the crack tip and it falls further — linearly, by outflow over a distance L, to atmospheric pressure — as it flares the released pipe wall.

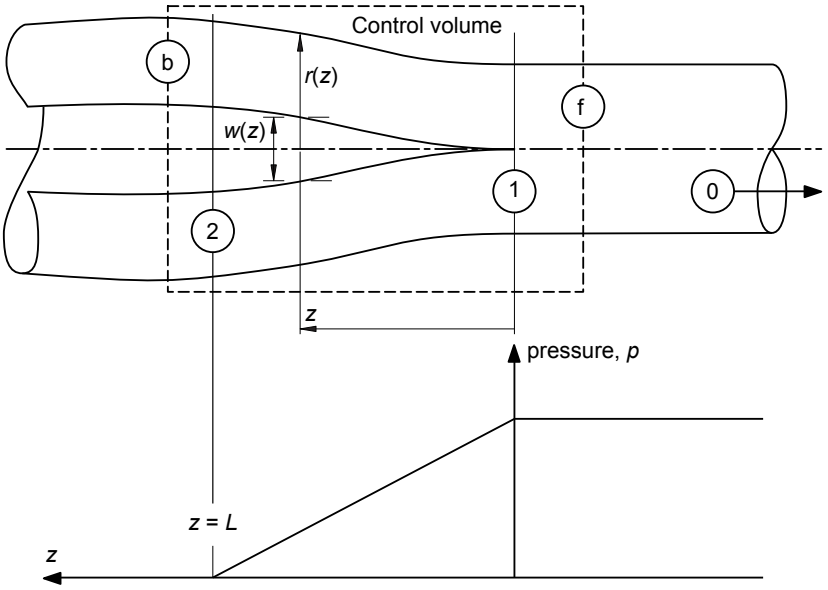


Figure 2: Pipe deformation and pressure distribution around the crack tip plane

To calculate G we apply the steady flow energy equation to a control volume surrounding, and moving with, the crack front. The chosen volume (Fig. 2) contains no pressurised fluid: its surface is wrapped onto the pipe bore and the fracture surface and cuts the pipe at two transverse planes. Strain g_{S} and kinetic g_{K} energies per unit length are carried in though the upstream plane by

the uncracked pipe wall and out through the downstream plane by the cracked but unpressurised pipe wall. The crack extension force is:

$$GB_{\mathrm{c}} = \frac{\mathrm{d}U_{\mathrm{E}}}{\mathrm{d}a} + [g_{\mathrm{S}} + g_{\mathrm{K}}]_{\mathrm{in}} - [g_{\mathrm{S}} + g_{\mathrm{K}}]_{\mathrm{out}} \tag{4}$$

where a is the crack length relative to the pipe, B_{c} is the crack path width (normally equal to the pipe wall thickness) and U_{E} is the pressure work done in the control volume.

3. Axial pressure distribution

There are two distinct regions [38] within the axial distribution of pressure around a propagating crack tip (Fig. 2), and for gas pressurisation simple models are available for both. Well upstream of the crack front, at plane 0, the contained fluid remains at its initial pressure p_0. Between there and the crack tip at plane 1 there is *decompression* by axial backflow. Downstream, there is *outflow* within the axial distance L between planes 1 and 2, at which ambient pressure p_{a} is restored.

3.0.1. Upstream decompression

Decompression is modelled [14] by one-dimensional flow towards a cross-sectional 'guillotine' cut at the virtual crack tip. The crack tip gauge pressure becomes

$$\left.\begin{array}{l} \frac{p_1+p_{\mathrm{a}}}{p_0+p_{\mathrm{a}}} = \left[1 - \frac{\gamma-1}{\gamma+1}\left(1 - \frac{\dot{a}}{c_0}\right)\right]^{2\gamma/(\gamma-1)}, z > 0,\ \dot{a} < c_0 \\ \frac{p_1+p_{\mathrm{a}}}{p_0+p_{\mathrm{a}}} = 1, z < 0,\ \dot{a} \geq c_0 \end{array}\right\} \tag{5}$$

where c_0 and γ are the decompression speed and specific heat ratio for the pressurising gas (for air, taken here as 330 ms^{-1} and 1.4 respectively). A first-order correction can be made to the Irwin-Corten expression by locating the front control surface boundary at plane 1 rather than plane 0, to yield

$$G_1 = \left(\frac{p_1}{p_0}\right)^2 G_0 \tag{6}$$

increasing the critical pressure by a factor p_0/p_1. Note that the essence of the S4 test is that decompression is suppressed by internal baffles, so that $p_1 \approx p_0$; this is the origin of the standard correlation equation (3).

3.0.2. Downstream outflow

Measurements at both full scale and small scale [15] suggest that the axial pressure profile is essentially linear, extending over a length L of 3–4 diameters. To predict L, Venizelos *et al.* [15] used the steady-state nature of RCP to transform the outflow process into an analogous transient problem: that of a

pressurised vessel, of volume V and initial gauge pressure p_1, discharging to ambient pressure p_a through an orifice of area A_t. Above a pressure ratio

$$\frac{p_1}{p_\mathrm{a}} = \left(\frac{\gamma+1}{2}\right)^{\gamma/(\gamma-1)} - 1$$

outflow is choked and the pressure decays as

$$p^* = \left[1 + \left(\frac{\gamma-1}{2}\right)\left(\frac{\gamma+1}{2}\right)^{\frac{-(\gamma+1)}{2(\gamma-1)}} t^*\right]^{\frac{-2\gamma}{(\gamma-1)}} \tag{7}$$

where $p^* = (p + p_\mathrm{a})/(p_\mathrm{i} + p_\mathrm{a})$ and $t^* = A_\mathrm{t} c_0 t/V$.

For lower pressures, outflow is unchoked and a closed-form solution is available [39, 40] only in the inverse form (for $\gamma = 7/5$):

$$t^* - t^*_\mathrm{unch} = \left(\frac{2}{\gamma-1}\right)^{1/2} (p^*_\mathrm{a})^{-\frac{\gamma-1}{2\gamma}} \left[\left(\frac{x^3}{4} + \frac{5}{8}x\right)\left(x^2+1\right)^{1/2} + \frac{3}{8}\ln\left(x + \left(x^2+1\right)^{1/2}\right)\right]_x^{x_\mathrm{unch}} \tag{8}$$

where

$$x \equiv \left[\left(\frac{p^*}{p^*_\mathrm{a}}\right)^{\frac{\gamma-1}{\gamma}} - 1\right]^{1/2}$$

The pressure/time characteristic from these equations is finally linearised and characterised by a discharge time:

$$t^*_\mathrm{disch} \equiv \frac{A_\mathrm{t} c_0}{V} t_\mathrm{disch} = \frac{2}{p}\int_0^T (p)\, dt \tag{9}$$

and A_t will be identified with the total crack opening area over the length L. The model neglects important features of each test configuration: for the FS test, the axial velocity of the gas near the outflow and for the S4 test, downstream leakage of air past the baffles. Better models exist for future development, e.g. that of Alder [38].

3.1. Deformation of the pipe wall

The components of a compatible displacement field for any pipe cross-section $z = \text{const.}$ are shown in Fig. 3. The unstrained pipe circumference is cut radially at, and 180° from the crack plane. After the sequence shown — axisymmetric expansion, lateral bending of the centroidal axis, torsion then vertical bending of the centroidal axis — the pipe is finally re-joined at $\theta = 180°$, leaving the crack surfaces at $\theta = 0$ separated by an opening of $w = 4R\phi$. Total displacements are:

$$u_r = \frac{1}{2\pi} w(z) \tag{10}$$

$$u_\theta = \frac{1}{2}\left(1 - \frac{\theta}{\pi}\right)\frac{r}{R} w(z) \tag{11}$$

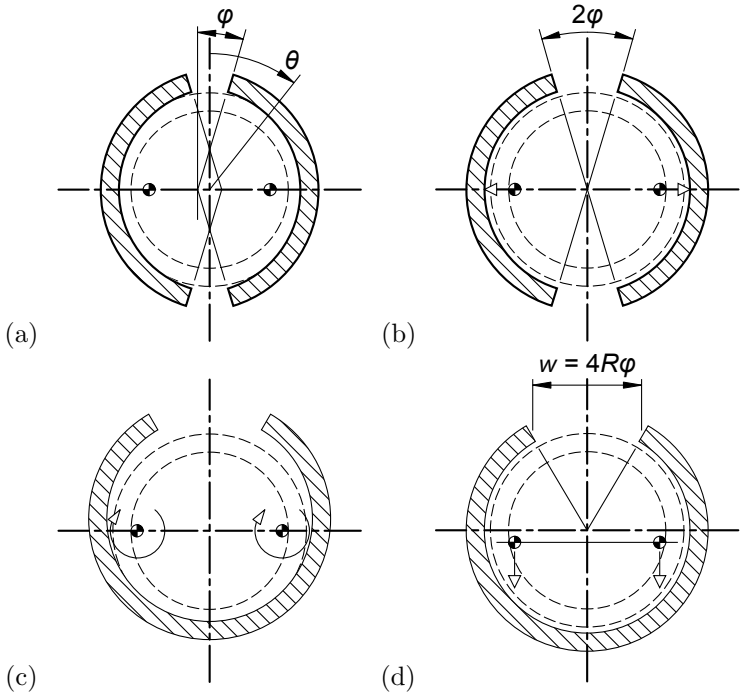


Figure 3: Deformation of one-half of the pipe cross-section: (a) radial expansion, without lateral displacement of the centroid (marked '+'); (b) lateral bending, returning the arc centre to the pipe axis; (c) torsion about the centroid, rejoining the pipe; and (d) vertical bending, returning the arc centre to the pipe axis.

and

$$u_z = \left[\left(\frac{4}{\pi^3} + \frac{\pi}{8} - \frac{\theta}{4}\right) R - \left(\frac{2}{\pi^2}\sin\theta - \frac{1}{2\pi}\cos\theta + \frac{\pi}{8} - \frac{\theta}{4}\right) r\right] w'(z) \qquad (12)$$

where $R = \frac{1}{2}D(D^* - 1)/D^*$ is the median radius.

The strain and kinetic energy densities generated at the front and back planes by this displacement field are derived in Appendix A. The work done per unit length by pressure forces acting through the inner surface of the control volume is $\frac{1}{2}p\,(2R - h)\,w$ at any section, amounting, for small displacements, to

$$\frac{\mathrm{d}U_\mathrm{E}}{\mathrm{d}a} = \frac{1}{2}\,(2R - h)\int_{z=0}^{L} p\,(z)\frac{\mathrm{d}w}{\mathrm{d}z}\,\mathrm{d}z. \qquad (13)$$

In order to evaluate this contribution to G, which will prove to be very large, the crack opening profile $w\,(z)$ must be determined. Before doing so we consider the role of residual strains.

3.2. Residual strains and their viscoelastic recovery

Locked into the wall of any melt-extruded thermoplastic slab cooled from both surfaces is a quasi-parabolic distribution of residual strain: tensile near the mid-wall, compressive on the surfaces. Conventional external-only pipe cooling unbalances this distribution, setting up in the wall inward bending moments both circumferentially and axially. In releasing the circumferential bending moment the crack effectively superimposes an equal and opposite one and the pipe, if unrestrained, curls viscoelastically to a diameter $D(t) < D$ by creep (Fig. 4). Any constraint due to overlapping (Fig. 4c) can be preempted by cutting a sector out. After waiting for a time t_creep at which a creep modulus $E(t_\mathrm{creep})$ is known, the *recoverable* residual strain can be characterised by measuring $D(t_\mathrm{creep})$. The linear strain profile of circumferential bending cancels out the original residual bending moment, although it cannot eliminate all of the quasi-parabolic residual strain.

Residual strain could affect RCP in two ways. Firstly, the strain energy released from states (a) to (d) of Fig. 4 could drive fracture — even, in principle, if the pipe were unpressurised. Secondly, additional pressure p_res0 is needed to overcome the force at the fracture surface contact line shown in Fig. 4(d). This modifies the crack opening and hence the outflow length.

Within the time scale of an RCP event only a fraction of the recoverable strain can be released, giving a less reduced diameter D_res0:

$$\frac{1}{D_\mathrm{res0}} = \left(1 - \frac{E(t)}{E_\mathrm{d}}\right)\frac{1}{D} + \frac{E(t)}{E_\mathrm{d}}\frac{1}{D_\mathrm{res\infty}}, \qquad (14)$$

where E_d is the value of $E(t)$ at the time scale t of the fracture process. If the pipe fractures without flaring, symmetry remains unbroken and the cross section is left in the state of Fig. 4d. The surfaces remain in contact along an axial line across which a circumferential surface traction F per unit length acts

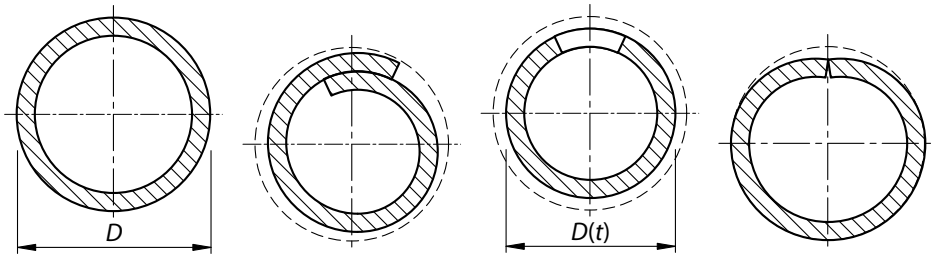


Figure 4: (a) Uncracked cross-section of a pipe with residual strain; (b) overlapping after fracture releases most of the available energy; (c) release of all available energy is physically prevented but (d) the only deformation mode possible during fracture releases most of it.

to prevent the overlapping of Fig. 4b. To calculate F, the method of Roark [41] is used to analyse a 180° segment of circular beam built-in at the end opposite the force. After some manipulation we find that the residual strain per unit length of pipe for Fig. 4d is:

$$\frac{\pi}{9}\frac{ED^2}{(D^*-1)^3}C_{\mathrm{D}}^2 \tag{15}$$

where the diametral contraction $C_{\mathrm{D}} = (D - D(t))/D$. The strain energy released by the total release of circumferential bending would have been

$$\frac{\pi}{6}\frac{ED^2}{(D^*-1)^2}C_{\mathrm{D}}^2$$

so that the net strain energy release per unit length becomes

$$g_{\mathrm{S}} = \frac{\pi}{6}\frac{ED^2}{(D^*-1)^2}C_{\mathrm{D}}^2\left[1 - \frac{2}{3\,(D^*-1)}\right]$$

which is almost all of that stored. If a crack could propagate along a pipe pressurised at

$$p_{\mathrm{res0}} = \frac{2}{3}\frac{E_{\mathrm{d}}}{D^{*3}}\left(1 - \frac{D_{\mathrm{res0}}}{D}\right) \tag{16}$$

the state of the pipe wall after the crack passed would resemble that assumed by Irwin and Corten: an approximately circular pipe cross section under zero hoop stress, with its cut surfaces in traction-free contact.

The effect of residual strain on the crack opening profile *behind* the crack can be represented either (as by Venizelos *et al.* [15]) as an external pressure p_{res0} or by increasing the crack opening to a virtual value

$$v = w + \pi\,(D - D_{\mathrm{res0}})\,. \tag{17}$$

Since $v' = w'$ etc., equations(A.5) and (13) are simply modified by replacing all w by v. The last term in (A.5) alone is sufficient to account for the greater energy needed, as a result of residual strain, to flare the pipe wall. However the portion of residual strain energy whose recovery is prevented by surface contact must be accounted for ahead of the crack, to preserve the energy balance (Eq. (4)). On doing so, (A.6) becomes

$$[g_{\mathrm{S}} + g_{\mathrm{K}}]_{\mathrm{in}} = \pi D^2 \left[\frac{p_1^2}{E_{\mathrm{d}}} \frac{(D^* - 2)^2 (D^* - 3)}{8 D^{*2}} + \frac{\pi}{6} E_{\mathrm{d}} \frac{1}{(6D^* - 1)^2} \right]. \qquad (18)$$

3.3. Backfill

The resistance of a gravel backfill to an expanding pipe can be characterised by a modulus of elasticity, a frictional yield stress (normally quoted as an equivalent angle of repose), a pressure (rather insignificant for the 0.1 m above an FS test pipe) and an inertial resistance due to its density ρ_{B}. For the time being we consider inertia alone. If the backfill can be assumed to be incompressible, the simplest kinetic model is that axisymmetrical expansion of the pipe wall drives 'point source' flow, giving it a radial velocity inversely proportional to radius. An axisymmetrical backfill sleeve of outside diameter D_{T} increases the pipe wall mass density from ρ to an effective value of

$$\rho \left[1 + \frac{\rho_{\mathrm{B}}}{\rho} \frac{D^*}{2} \left(\frac{D_{\mathrm{T}}}{D} - 1 \right) \right]. \qquad (19)$$

4. Formulation and solution as an equivalent simple beam

Translation via Eq. 17 from physical (w) to virtual (v) crack surface opening displacement does not change the dependency of any strain or kinetic energy term on the axial variable z. These dependencies are precisely those for the deflection v, under an applied pressure distribution, of a uniform, simple beam, mounted an elastic foundation and emerging at constant speed from a fixed reference point. Appendix B analyses this beam model, following Williams (1998), to express the beam width, cross sectional area, second moment of area, density and foundation modulus in terms of the pipe dimensions and properties. Their values carry clear physical meaning: e.g. the foundation modulus is very low because it represents relative diameteral expansion of a cracked, pressurised tube.

The full beam-on-elastic-foundation model can be represented as shown in Fig. 5. The beam, mounted on rollers through linear springs, is extruded horizontally at constant speed $\dot{a}$ from the crack front point and immediately meets a linearly decreasing downward pressure. There is no crack opening displacement: the springs do not represent, as in [37], a crack-tip line-spring array. Residual strain is represented simply as a downward displacement of both the extrusion point and the closure point, which correspond respectively to states (a) and (d) in Fig. (4), leaving the support springs pre-compressed outside the solution

zone. Also shown on Fig. 5 is the point at which downward (i.e. opening) acceleration of the beam ceases: this is where any backfill (not shown) will lose contact with the pipe and fly off downwards. We account both for the resulting local change in effective beam density and, in G calculation, for the kinetic energy of the ejected backfill [15].

Appendix B goes on to reduce the governing simple beam equation and its parameters to standard, dimensionless form: Eq. (B.12). It no general analytical solution, but a useful reference solution within $0 < \zeta < 1$ can be obtained by neglecting the support term in m. For the linear pressure profile $f(\zeta) = (1 - \zeta)$, and for boundary conditions $v^*(0) = v'^*(0) = 0$ and $v''^*(1) = v'''^*(1) = 0$, this is:

$$v^* = \frac{1}{\alpha^2}\left[\frac{1}{2}\zeta^2 - \frac{1}{6}\zeta^3 + \frac{1}{\alpha^2}\left(\zeta\cos\alpha - \frac{1}{\alpha}\sin\alpha\right) + \frac{1}{\alpha^3}\sin(1-\zeta)\,\alpha\right]. \qquad (20)$$

The full solution should match Eq. (20) in the near-tip region where the crack opening is small and the elastic foundation has little influence.

Williams [36] used this solution and treated the beam dimensions as fitting parameters for data, but the values required were rather non-physical and the dependence on decompression length became unbounded. An unpublished draft of the present model derived the parameter values analytically and attempted to correct for the support stiffness by accounting for it in the energy balance. Zhang [29] attempted to further correct that solution using a least-squares method but did not account for m in the boundary conditions as well as in the solution interval. The analytical formulation of Kanninen *et al.* [6] yielded a governing equation similar in form to Eq. (B.12) but the physical meaning of the parameters was different, because while plastic deformation was accounted for, the foundation stiffness represented backfill elasticity alone.

We solve Eq. (B.12) using a simple finite-difference method. First, Equation B.13 is used to calculate α from crack speed and B.14 to calculate m from pipe properties. A few tens of $v*$ nodes are set and boundary conditions of zero displacement and gradient are applied at the crack front and at the closure point to which the springs return the beam. Using LU decomposition the coefficient matrix is solved iteratively with two constraints:

1. The closure point position — initially placed at about 2 outflow lengths from the crack tip, and iterated for zero local bending moment so that conditions downstream will not affect the solution region; and
2. The outflow length — initially chosen at about 3 diameters, and iterated for equality with the product of crack speed and outflow time (here calculated using Eq 9).

5. Results and discussion

Figure 6 compares our results with those from O'Donoghue *et al.* [7] for a PE pipe of 300 mm diameter, SDR 16.5 and assumed modulus 2.07 GPa.

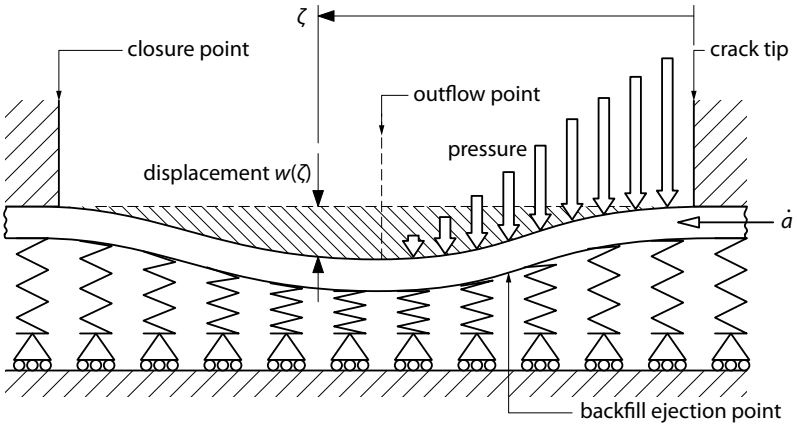


Figure 5: The pipe model expressed as an equivalent dynamic 'beam on elastic foundation' deflecting under pressure. The shaded area represents the crack opening, which controls outflow.

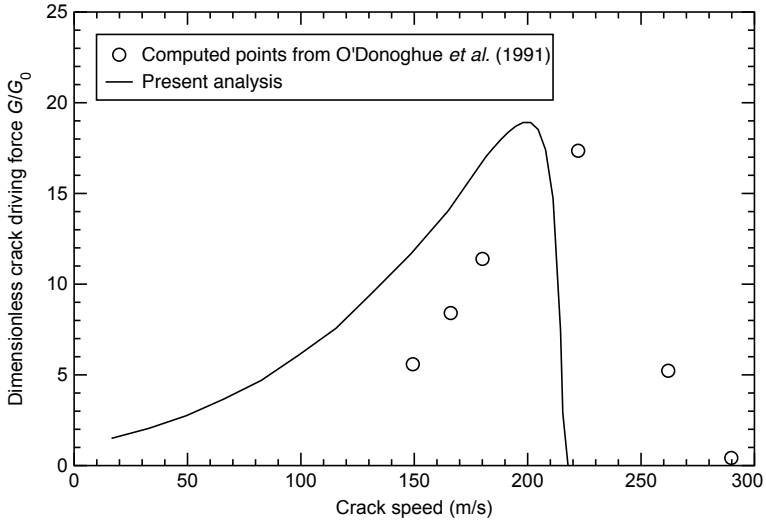


Figure 6: Comparison of results from the present model with those of O'Donoghue *et al* [7] for a non-backfilled 300 mm diameter SDR 16.5 PE pipe with $E_{\mathrm{d}} = 2.07$ GPa at 6.2 bar.

O'Donoghue's results are shown as points and they are sparse, reflecting the computing effort involved but making it difficult to estimate the peak. The overall similarity is encouraging and the all-important peak G values agree well. However, the shift of our $G(\dot{a})$ curve to lower velocities suggests an underestimate of the system stiffness and/or an overestimate of the kinetic energy, and is apparently an artifact of our simple model: we have seen cracks propagate in S4 tests at velocities beyond that of the abrupt G cutoff, and approaching the limiting speed predicted [42] on theoretical grounds:

$$\dot{a}_{\max} = \frac{3}{4}\sqrt{\frac{E_{\mathrm{d}}}{(D^* - 1)\rho}} \tag{21}$$

Nevertheless, for the non-backfilled FS test quoted [20] as support for the finite-element model, ours would have predicted exactly the same result: propagation at about 200 m/s. Furthermore, comparing our results with those from the finite-volume analysis based method of Ivankovic, Greenshields and co-workers [33] (Fig. 7) points us in the opposite direction. The disparity in peak G values here is greater, but ours would lead to a more conservative prediction of critical pressure — and only by 9%.

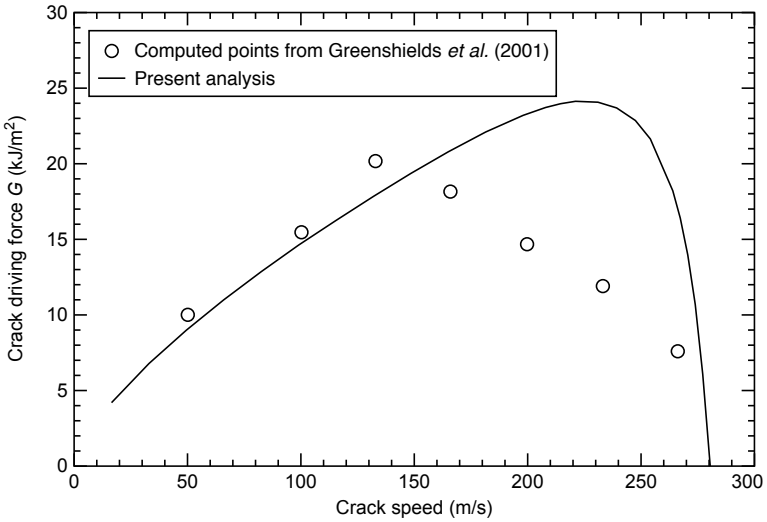


Figure 7: Comparison of results from the present model with those of Greenshields *et al.* [33] for an S4 test on 160 mm diameter SDR 11 PE pipe with $E_{\mathrm{d}} = 2.5$ GPa at 4.0 bar.

5.1. Crack opening profile

In earlier work Leevers and co-workers treated fracture as a local, high-rate process and used dynamic modulus E_{d} values determined ultrasonically at 1 MHz [9]. These values were high: typically 2.6 GPa for PE80 and 3.2 GPa

for PE100 at 0°C. We now recognise that since most of the fracture energy is associated with flaring, the relevant timescale is $L/\dot{a}$: a few milliseconds. Relevant test frequencies of a few hundred Hz are accessible using dynamical spectroscopy, and give modulus values typically 50% lower.

When the outflow length and closure point have relaxed to convergence, the finite difference procedure delivers a physical crack opening profile $w(z)$. Figure 8 compares $w(z)$ with one frame from a high-speed video used to measure it. The model provides insight into the S4 test and its suspected shortcomings. Simulations at the test temperature of -24°C, at which $E_{\rm d} = 1.7$ GPa, and are shown both neglecting and accounting for residual stress (which closed the pipe by 10% after creep). The crack opening profile is quite well predicted given that the crack has reached the end-cap whilst the predicted closure point lies beyond the initiation end of the specimen. We attribute the excess flaring to backflow leakage from upstream chambers which are supposedly separated by internal disc baffles (whose edges are visible through the crack in the photo as white lines) but which in fact allow leakage even within the uncracked length. Subsequent frames show that after the crack enters the specimen endcap — which, being external, clamps it shut — the last chambers exhaust into those behind and further flare the pipe. The model seems to suggest that the S4 test specimen is too short.

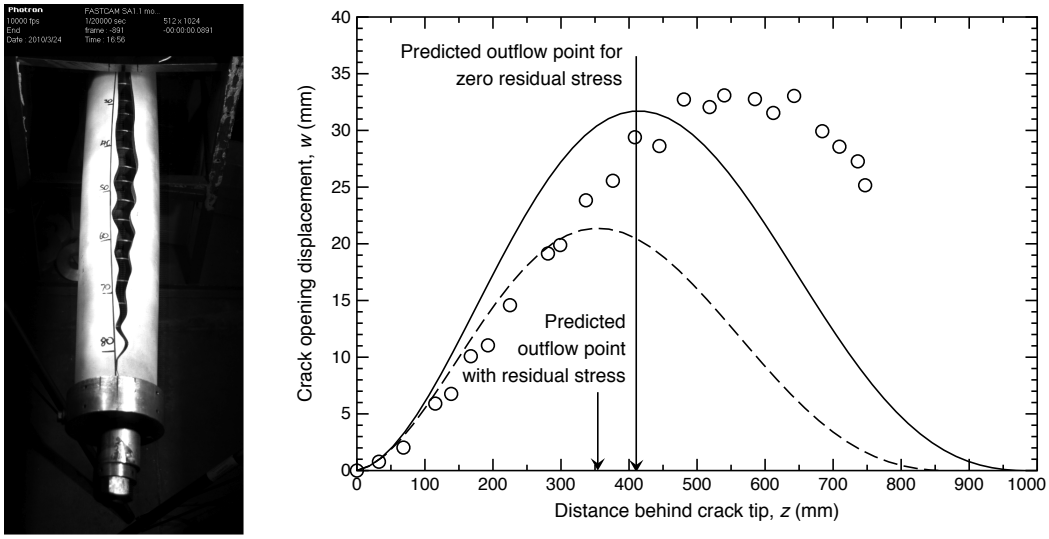


Figure 8: Crack opening profiles: (left) seen in a high-speed video frame from an S4 test on 125 mm SDR11 PE100 pipe at -24°C, and (b) plotted (points) with simulated lines (with and — dashed — without residual stress).

But does this matter? Figure 8, like all subsequent results in this paper, is computed for a generic PE at 0°C, and with $E_{\rm d} = 1.5$ GPa. Integrating the

pressure work (which provides a large proportion of G) through the outflow zone reveals its axial distribution, as shown in Fig. 9 for low and high crack speeds. Figure 9 shows clearly that when the pressure has fallen by 50%, about 85% of the work has already been done. For this reason the outflow length is calculated by doubling this time, rather than using Eq. (9).

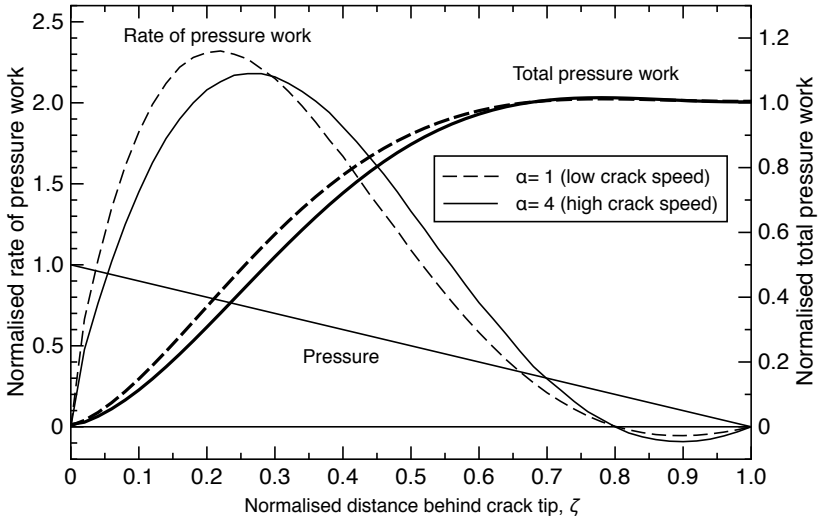


Figure 9: The distribution of pressure work U_{E} within the outflow zone for low and high values of normalised crack speed α

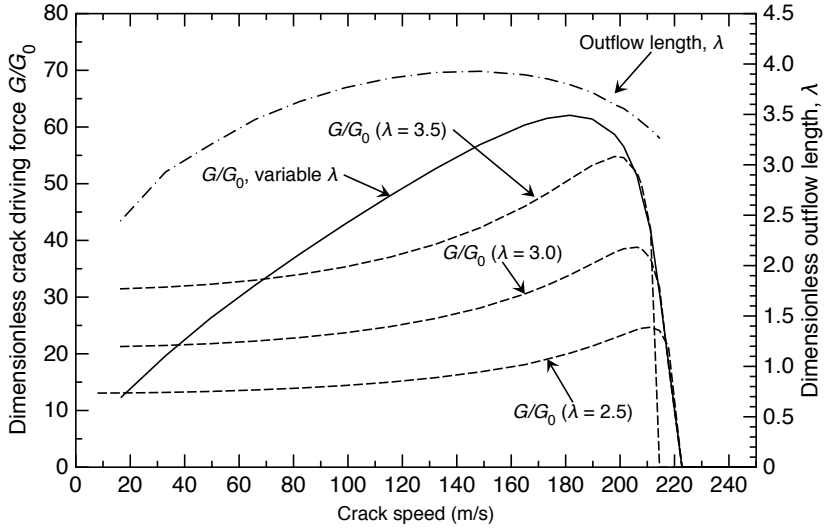
5.2. Effects of pipe size, crack speed and outflow length

As a baseline to demonstrate the model we choose 250 mm SDR 11 pipe — a size commonly tested using both S4 and full-scale methods — and a generic PE with $E_{\mathrm{d}} = 1.5$ GPa. Figure 10 presents G/G_0 results as a function of crack speed at test pressures of 1.5 bar (S4) and 5 bar (FS). The static discharge outflow model is used to determine outflow length $\lambda = 2L/R$, but G/G_0 values are also plotted for a few constant λ values in the range it predicts.

Figure 11 shows the various components of the fracture energy balance for S4 tests at low (1.5 bar) and high (5 bar) pressures. At typical crack speeds the Irwin-Corten component itself — against which the others are normalised — hardly registers in comparison to the pressure work. Although the pipe wall inertia plays a significant role in the system mechanics, only at speeds immediately approaching the $G = 0$ cut-off does kinetic energy decisively influence the overall balance. The cut-off speed is strongly influenced by modulus: using the ultrasonic modulus referred to above restores it almost to sonic velocity.

For constant pipe shape (i.e. standard dimensional ratio, SDR) this model predicts the crack driving force to be independent of pipe diameter. The effect

(a)



(b)

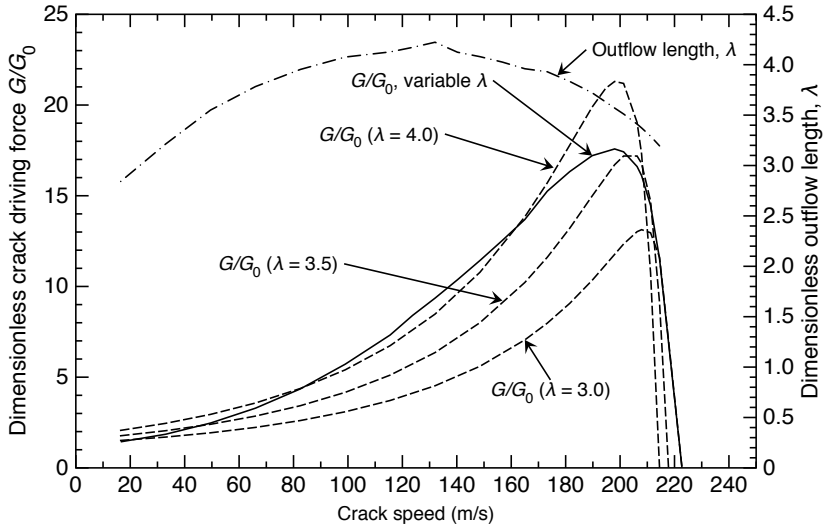
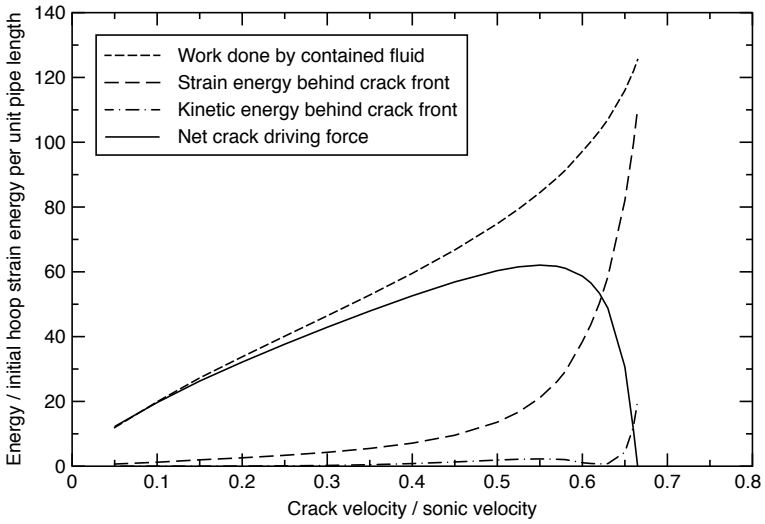


Figure 10: RCP driving force G and outflow length in mean diameters, for RCP tests on 250mm SDR11 generic PE pipe at 0°C. (a) S4 method at 1.5 bar ($G_0 = 0.1084$ kJ/m^2). (b) FS method at 5 bar ($G_0 = 1.205$ kJ/m^2).

(a)



(b)

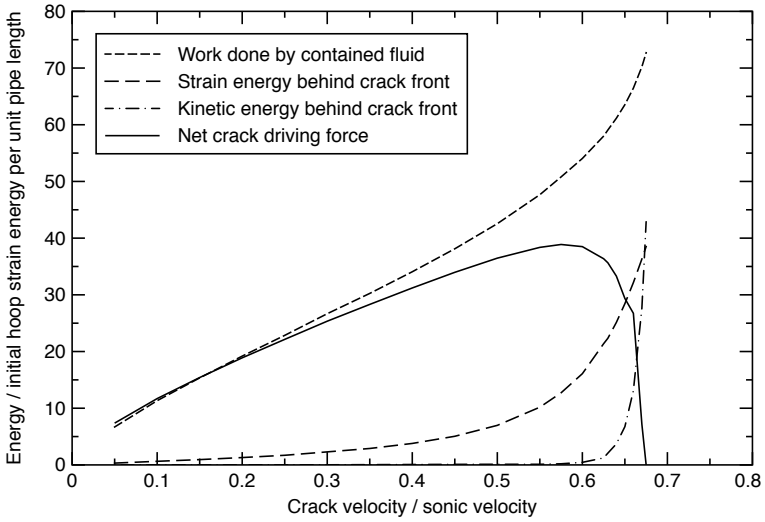


Figure 11: (a) Components of energy (per unit length, normalised against Irwin-Corten value g_0) in 250 SDR 11 PE pipe during RCP in an S4 test configuration.

of thickness at constant diameter is illustrated in Fig. 12. For this thinner pipe both the normalised peak driving force G/G_0 and the speed at which it is delivered are considerably reduced. Both effects will increase the critical pressure, since at this lower speed PE is beginning to show more resistance to plane strain RCP [10].

5.3. Effect of test pressure

A persistent issue of S4 testing is the *cloche* (bell curve) effect: short crack lengths at low-pressure arrest become long crack lengths defining 'propagation' results at intermediate pressures, as expected — but revert to short crack lengths at higher pressures. Figure 11 already shows that although the effect of pressure on crack driving force G should have been factored out by normalising against g_0 (Eq. (1)), there is a secondary decrease of 35% on increasing the pressure from 1.5 to 5 bar.

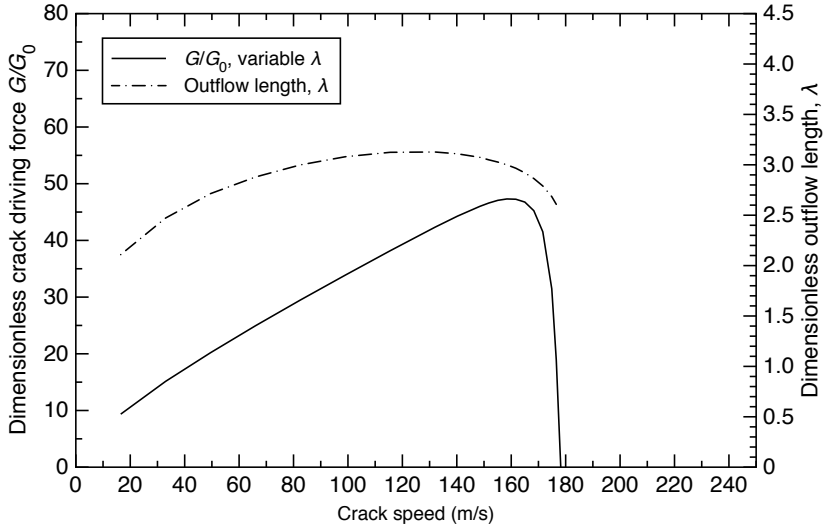
The broader picture is shown in Figure 13. The computed *peak* G/G_0 and the corresponding outflow length both decrease while the velocity at the peak G increases slightly. As pressure is increased, outflow is increasingly choked and the gas can contribute progressively less to driving the crack. The decrease in G/G_0 is not nearly enough to counter the increase of G_0 itself and explain high-pressure arrest. However, the computed diametral expansion of the pipe at the critical maximum-G condition is also plotted, and this provides a more credible explanation. ISO 13477 requires a containment cage of concentric rings to restrict radial expansion of the pipe circumference, during fracture, to within $(1.1 \pm 0.04D)$. *Cloche* effects have not been reported below 5 bar, and this is the pressure at which the computed maximum predicted pipe diameter during flaring reaches the inside surface of the smallest standard S4 cage. Pipe-cage contact will reduce the crack driving force because even if the restricted crack opening delays outflow of the pressurising air, this air can no longer help to drive the crack.

It was shown above that the displacement profile $w(z)$ exerts most influence on the G solution in the near-tip half of the outflow region. For this reason, the outflow length is determined from the outflow model pressure history by extrapolation from the time for 50% pressure drop. For low pressures (1–2 bar) the pressure decay is very linear and this is about 50% of the total outflow time; for high pressures (> 5 bar) it is less, because outflow is initially more rapid.

The predicted outflow length L is, especially at low pressures, very long compared to the S4 specimen gauge section — and the natural closure point is typically more than $2L$. Clearly, the specimen end cap must influence the crack opening profile and hence the crack driving force. The S4 test was designed empirically to shorten these axial dimensions, but the model tells us that the the specimen may not now be long enough. Crack arrests in the nominally 'steady state' region of the gauge length are not uncommon in some materials. Another factor presently unaccounted for in the S4 model is the influence of leakage over the baffles in the outflow zone.

The full scale test configuration has its complications too, and the model will now be used to investigate them.

(a)



(b)

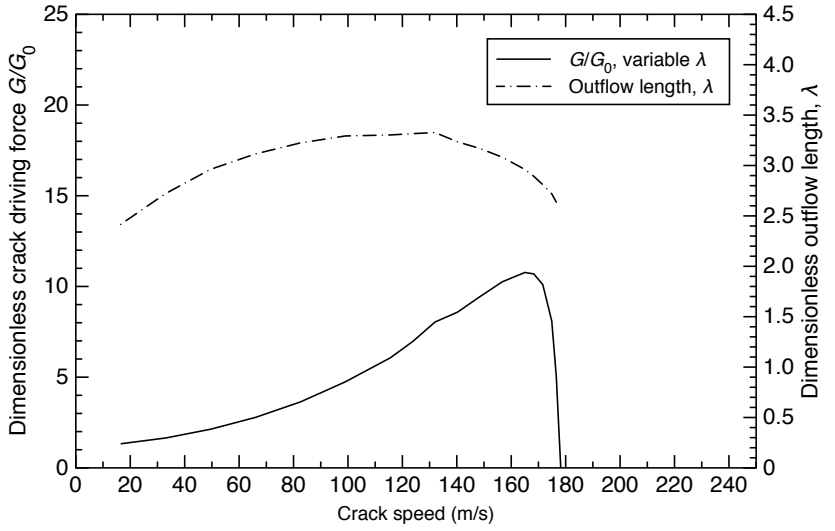


Figure 12: RCP driving force G and outflow length in mean diameters, for RCP tests on 250mm SDR17.6 generic PE pipe at 0° C. (a) S4 method at 1.5 bar ($G_0 = 0.1084$ kJ/m^2). (b) FS method at 5 bar ($G_0 = 1.205$ kJ/m^2).

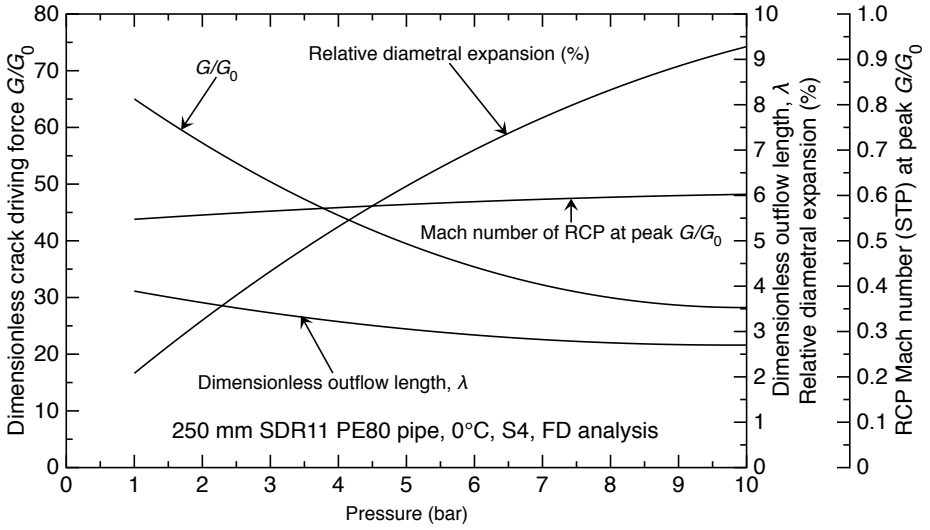


Figure 13: Effect of S4 test pressure on 250mm SDR11 PE pipe at 0° C.

5.4. Effects of backfill constraint

A typical S4 critical pressure for 250 SDR 11 PE80 pipe is 1.3 bar. Using the results of Fig. 10(a) yields $G_{\rm d} = (1.3/1.5)^2 \times 62 \times 0.1084 = 5.13$ kJ/m^2, a credible value. However, if $G_{\rm d}$ is assumed to be equal in both cases (i.e. one assumption, amongst others, is that the $G_{\rm d}(\dot{a})$ characteristic is flat), Fig. 10(b) can be used to back-calculate an FS critical pressure as shown in the schematic of Fig. 1:

$$p_{\rm cFS} = \sqrt{\frac{62.3}{17.1} \times \frac{0.1084}{1.205}} \times 5 = 2.86 \text{ bar}.$$

This seems too low, i.e. the G computed for the full-scale test appears to be unrealistically high.

Full-scale RCP tests dramatically demonstrate the energy ejected from the pipe trench with the backfill, and the model of Section 3.3 now provides confirmation. For developers of the FV model low G results for FS test simulations were also a problem until backfill KE was accounted for [15]. The $G(\dot{a})/G_0$ curves for 110 and 250 mm pipe of the same SDR are identical, the diameter effect appearing in G_0. For an FS test with inertial loading from a coaxial backfill sleeve of wet gravel (density 2200 kg/m^3) 100 mm thick, this being the minimum required top cover depth, G is barely affected. Increasing the jacket thickness just to 150 mm, however, reduces the $G(\dot{a})/G_0$ peak from 17.1 to 10.9 and increases the predicted critical pressure by a factor $\sqrt{17.1/10.9}$ to 3.6 bar. This prediction remains lower than the 6 bar critical pressure for PE80 reported by Greig [16], but the backfill properties unaccounted for — frictional resistance and pressure — will increase it. More significantly, the crack speed at which the peak driving force is delivered has decreased from 200 to about 160 m/s. As

suggested in the schematic of Fig. 1, as crack speed decreases through about 150 m/s G_{d} for PE begins to climb, requiring a further increase in pressure. Finally, as will be argued in a forthcoming paper, the asymmetry of the RCP crack front in pipe leads to a substantial increase in toughness with pressure.

For 110 mm pipe, the decrease in crack driving force and in the peak driving force and in the expected crack speed are substantial even for 100 mm backfill jacket. To validate the backfill model, earlier experiments using the S4 method [23] were simulated. These showed that for a 110 mm SDR11 PE80 pipe whose S4 critical pressure p_{cS4} was 1.65 bar, dry, loosely compacted backfill increased p_{cS4} to 2.0 bar. Our simulations predicted an increase from 1.65 to 2.1 bar, showing agreement to within the resolution of the test. These results suggest that the ISO 13478 full-scale RCP test may be influenced as much by the presence and nature of the backfill as by the quality of the pipe. Although the method is designed to test the product 'as installed', it seems that a more careful investigation of the role of backfill and characterisation of its properties is needed.

Kanninen *et al.* [6] did observed that backfill substantially decreased crack speeds even in steel linepipe. Having modelled backfill as a purely elastic constraint and seen little effect on G, they concluded that the crack was overdriven (as by the upper 'bell curve' of Fig. 1) and that the presence of backfill had in some way stabilised the left-hand intersection. For plastic pipe the issue can only be settled by testing at full scale without backfill — which Grigory [21] advocated on the grounds not only of interpretative convenience but also of cost. S4 tests on large pipe may be at least as difficult and expensive as FS tests to which they were promoted as an economical alternative; the S4 test was, indeed, originally developed as a research tool rather than a pipe specifying method. Kanninen and Grigory's group had already demonstrated the feasibility of this method [20] but completed just one test at a pressure appropriate to buried, not unburied plastic pipe. The evidently overdriven crack did not propagate in the stable manner assumed by steady-state RCP analysis, but bifurcated to cause pipe fragmentation and self-arrest. The present analysis suggests trying again, at a considerably lower pressure.

5.5. Effects of contained water

The effects of pressurisation by water-air mixtures, too, can be modelled by attaching equivalent mass to the pipe wall. Experimental results were obtained by Greenshields [43] using a modified S4 test in which the internal volume of the reference uncracked, unpressurised pipe contained not only a rigid volume fraction allowed by the S4 test standard $\chi_{\mathrm{S}} \leq 0.25$ but also an incompressible fluid (e.g. water) volume fraction χ_{L} (Fig. 15(a)). The remaining gas content ($\chi_{\mathrm{G}} = 1 - \chi_{\mathrm{S}} - \chi_{\mathrm{L}}$) flares most of the fractured pipe wall *via* the water, so that to drive a crack it must move both masses. Note that if $\chi_{\mathrm{G}} = 0$ and the crack velocity can exceed the Joukovsky wave velocity for the pipe/fluid system, the critical pressure can be determined independently *via* the Irwin-Corten solution [35].

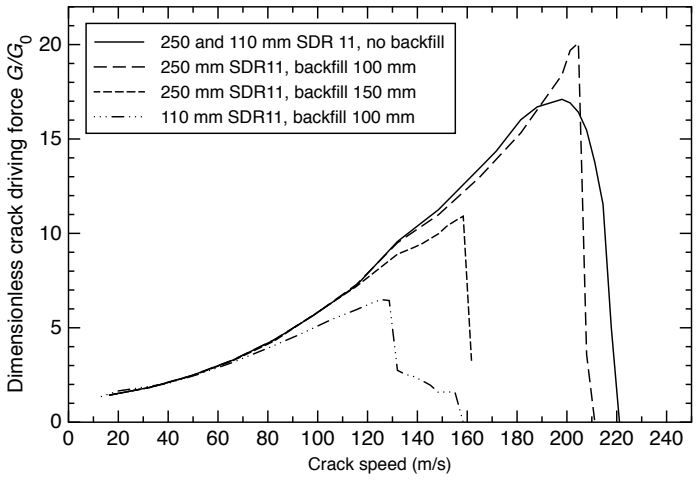


Figure 14: RCP driving force for open and backfilled FS tests at 5 bar on 110mm ($G_0 = 0.5301$ kJ/m^2) and 250mm ($G_0 = 1.205$kJ/m^2) SDR11 PE pipe

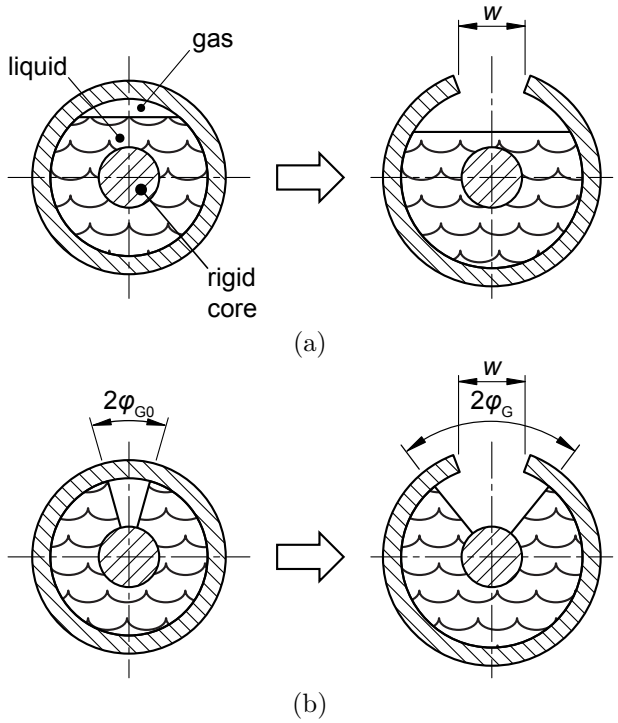


Figure 15: (a) A water-air-pressurised S4 pipe before and during fracture, kinetically modelled (b) using an expanding 'gas sector'

The effective mass of liquid 'attached' to the pipe wall is estimated using the simple model of Fig. 15(b). The rigid content is lumped into a central coaxial core of diameter R_S and the gas is assumed to occupy a segment bounded by radial lines subtending an angle $2\phi_{\mathrm{G}0}$. Thus the volume per unit length of liquid (assumed incompressible) is $(\pi - \phi_{\mathrm{G}0})(R_\mathrm{i}^2 - R_\mathrm{S}^2)$, and if axial flow is neglected while the pipe bore expands from its internal radius R_i to R then

$$(\pi - \phi_\mathrm{G})\left(R^2 - R_\mathrm{S}^2\right) = (\pi - \phi_{\mathrm{G}0})\left(R_\mathrm{i}^2 - R_\mathrm{s}^2\right) \tag{22}$$

where $R = R_\mathrm{i} + v/2\pi$. The initial gas sector angle is

$$\phi_{\mathrm{G}0} = \pi \frac{\chi_\mathrm{G}}{\chi_\mathrm{G} + \chi_\mathrm{L}} = \pi \left[1 - \frac{\chi_\mathrm{L}}{1 - \chi_\mathrm{S}}\right]. \tag{23}$$

Hence, since $\chi_\mathrm{S} = (R_\mathrm{S}/R_\mathrm{i})^2$:

$$\phi_\mathrm{G} \left[\left(1 + \frac{v}{2\pi R_\mathrm{i}}\right)^2 - \chi_\mathrm{S}\right] = \phi_{\mathrm{G}0}\left(1 - \chi_\mathrm{S}\right) + \frac{v}{R_\mathrm{i}}\left(2 + \frac{1}{2\pi}\frac{v}{R_\mathrm{i}}\right) \tag{24}$$

yielding the gas sector opening rate in terms of the pipe wall velocity. A simple velocity field which satisfies these boundary conditions but satisfies continuity only at the global level is:

$$\dot{u}_r = \frac{\dot{v}}{2\pi}\frac{r - R_\mathrm{S}}{R_\mathrm{i} - R_\mathrm{S}} \tag{25}$$

$$\dot{u}_\theta = \dot{\phi}_\mathrm{G} r \frac{\pi - \theta}{\pi - \phi_{\mathrm{G}0}} \tag{26}$$

Calculating the kinetic energy per unit length

$$\rho_\mathrm{water} \int_{\phi_{\mathrm{L}0}}^{\pi} \int_{R_\mathrm{S}}^{R_\mathrm{i}} \left(u_r^2 + u_\theta^2\right) r \mathrm{d}r\mathrm{d}\theta \tag{27}$$

yields both the effective mass of water moving at speed $\dot{w}$ (which is a function of w) and the kinetic energy value at plane 2 (Fig. 2) for the energy balance.

To keep this indicative analysis tractable we just compute these quantities, finding that the velocity ratio for $\chi_\mathrm{s} = 0.25$ to be well described as

$$\dot{\phi}_\mathrm{G} = \frac{1}{4\pi R_\mathrm{i}}\left[\frac{50}{3} - \frac{200}{9}\chi_\mathrm{G}\right]\dot{v} \tag{28}$$

Figure 16 show the results for the case studied by Greenshields, showing remarkably close agreement. This result further supports the emphasis given above to mass density, rather than frictional resistance or hydrostatic pressure, when analysing the effects on RCP of backfill.

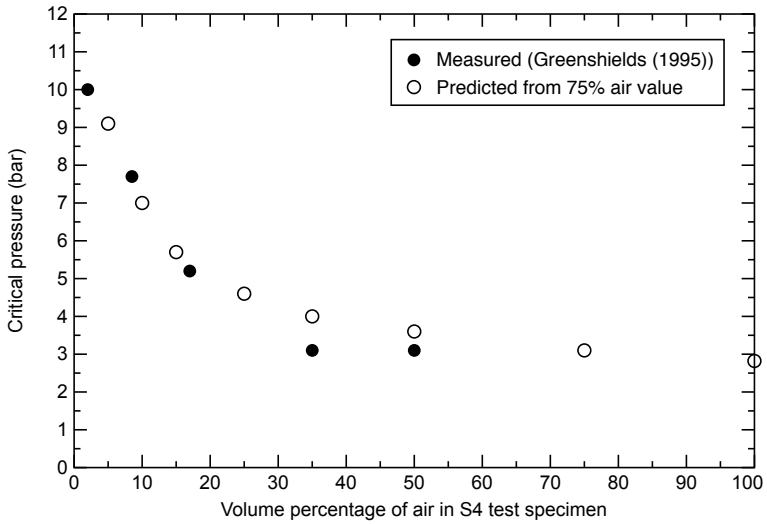


Figure 16: Data from Greenshields water/air-pressurised S4 pipe RCP tests, with values simulated from the air-pressurised test result.

5.6. Effects of residual strain

Due to residual strain, the diameter of PE pipe may contract after fracture (Fig. 4) to less than $0.9D$, revealing residual stress levels which are a significant proportion of the working stresses. However, this simple model — which in other respects has significantly improved our understanding of RCP test configurations — reveals no significant effects of residual stress on the driving force. The results are in fact consistent with those from earlier modellers [15]. The predicted effects on G are relatively small even for the low pressures used in S4 tests. In response to the crack-closing effect of residual strain, the outflow length increases and the effect on G depends both on pipe material modulus and on backfill depth. The increased initial strain energy appears in G at low speeds in the full-scale test at modest pressures (5 bar); as speed increases and pressure work dominates, G is reduced by the downstream 'negative pressure' effect of residual stress.

It seems more likely that the observed effect of residual strain on RCP in PE pipe can be understood through its effect on crack shape [26]. At present the analysis (unlike that of Ivankovic *et al.* [44]) assumes a straight, through-thickness front. Crack curvature reduces the average crack velocity [45] and for RCP in plastics this can substantially increase the dynamic fracture resistance.

6. Conclusions

The plastic pipe industry needs an accessible model for virtual RCP tests. We have developed a system, built around a relatively simple semi-analytical

model, which seems to work well and whose modular form should facilitate further experimentation. Simulations throw light on issues concerning both S4 test (whose gauge length may be too short and whose containment cage is probably responsible for the *cloche* effect) and the full-scale test (which may be excessively sensitive to backfill type and depth). Residual strain may affect pipe performance marginally for low-modulus or high-SDR pipe at the low pressures used in the S4 test, and less in the FS test. Overall, the success of the standard FS/S4 correlation factor now appears to be somewhat fortuitous.

7. Acknowledgements

Much of the groundwork for this model was completed during the 1990s with long-running support from the UK Engineering and Physical Sciences Research Council. The author wishes to express special appreciation to Chris Argyrakis for resuscitating the model during his PhD project, and to Repsol YPF for funding him to do so.

Appendix A. Derivation of strain and kinetic energy densities in the flaring pipe wall

Circumferential strains set up in the wall opposite the crack, and shear strains set up in the shell plane by torsion of each half-section, are neglected; the place of shear strains in the solution is kept by the torsional component only. Calculating strains and strain energies we arrive finally at:

$$g_{\mathrm{Sout}} = \frac{1}{2}E\left[\frac{1}{24\pi}\left(\frac{h}{R}\right)^3 w^2 + C_1 R^3 h w''^2\right] + \frac{\pi}{48}\mu R h\left(\frac{h}{R}\right)^2 w'^2 \tag{A.1}$$

Under steady-state conditions, displacement rates can be expressed in terms of axial displacement gradients: $\dot{w} = \dot{a}w'$, where a dot denotes a time derivative. Point velocities are

$$\left.\begin{array}{l} \dot{u}_r = \dot{a}\frac{w'}{2\pi} \\ \dot{u}_\theta = \dot{a}\left(1 - \frac{\theta}{\pi}\right)\frac{w'}{2} \\ \dot{u}_z = \dot{a}q\left(\theta\right)Rw'' \end{array}\right\} \tag{A.2}$$

where $q\left(\theta\right) = \frac{4}{\pi^3} - \frac{2}{\pi^2}\sin\theta + \frac{1}{2\pi}\cos\theta$.

The total kinetic energy density is

$$g_{\mathrm{Kout}} = \frac{1}{2}\rho\int_{\theta=0}^{2\pi}\int_{R-h/2}^{R+h/2}\left(\dot{u}_r^2 + \dot{u}_\theta^2 + \dot{u}_z^2\right) r\,\mathrm{d}r\,\mathrm{d}\theta \tag{A.3}$$

which, on neglecting through-thickness velocity gradients, amounts to

$$g_{\mathrm{Kout}} = \frac{1}{2}\rho R h\dot{a}^2\left(C_2 w'^2 + C_1 R^2 w''^2\right) \tag{A.4}$$

where

$$C_1 = \frac{1}{4\pi} + \frac{4}{\pi^3} - \frac{32}{\pi^5} = 0.10402$$

and

$$C_2 = \frac{\pi}{6} + \frac{1}{2\pi} = 0.68275$$

The total internal energy per unit pipe length within $z > 0$ is therefore

$$\begin{aligned} g_{\mathrm{S}} + g_{\mathrm{K}} &= \tfrac{1}{2} E C_1 R^3 h \left[1 + \left(\tfrac{\dot{a}}{c_{\mathrm{L}}}\right)^2\right] w''^2 \\ &+ \tfrac{1}{2}\mu R h \left[\tfrac{\pi}{24}\left(\tfrac{h}{R}\right)^2 + C_2\left(\tfrac{\dot{a}}{c_{\mathrm{S}}}\right)^2\right] w'^2 + \tfrac{1}{48\pi} E \left(\tfrac{h}{R}\right)^3 w^2 \end{aligned} \tag{A.5}$$

where $c_{\mathrm{L}} \equiv (E/\rho)^{1/2}$ and $c_{\mathrm{S}} \equiv (\mu/\rho)^{1/2}$ are the longitudinal and shear elastic wave speeds in the pipe material.

Ahead of the crack front, the internal energy of the pipe wall consists mainly of strain energy due to pressure loading. If the depressurisation zone is long, kinetic energy can be neglected. Thus

$$[g_{\mathrm{S}} + g_{\mathrm{K}}]_{\mathrm{in}} = \frac{\pi p_1^2}{E} \frac{(2R-h)^2 (R-h)}{4h} \tag{A.6}$$

as in the Irwin-Corten model.

Appendix B. Derivation *via* the BOEF model of model parameters in terms of physical parameters

For a simple beam of cross-sectional area A and second moment of area I, deflecting by v from an elastic foundation of stiffness M per unit length under an applied pressure distribution $p(z)$ acting on a projected area W per unit length, the equation of motion is:

$$EI\frac{\mathrm{d}^4 v}{\mathrm{d}z^4} + \rho A \frac{\mathrm{d}^2 v}{\mathrm{d}t^2} + Mv = W p(z)\,. \tag{B.1}$$

If the beam separates from a rigid base at a point $z = 0$ which translates at constant velocity $\dot{a}$, the steady state profile in $z > 0$ is governed by

$$EIv^{(4)} + \rho A \dot{a}^2 v'' + Mv = W p(z) \tag{B.2}$$

Within this region, the total dynamically-recoverable elastic strain energy and kinetic energy per unit length are

$$g_{\mathrm{S}} = \frac{1}{2} E_{\mathrm{d}} I v''^2 + \frac{1}{2} M v^2 \tag{B.3}$$

and

$$g_{\mathrm{K}} = \frac{1}{2}\rho A \dot{a}^2 v'^2 \tag{B.4}$$

Since the work done per unit length by pressure is pWv, the total rate of external work is

$$\frac{\mathrm{d}U_{\mathrm{E}}}{\mathrm{d}a} = W \int_0^L p(z) v' \,\mathrm{d}z \tag{B.5}$$

The pipe model can therefore be represented in this dynamic beam-on-elastic-foundation form by equating internal energy and external work terms which have equivalent dependence on the displacement function $v(z)$. On comparing Eqs. (B.3) and (A.5) an effective second moment of area I is defined through

$$I = \frac{1}{8} C_1 \left(\frac{D}{D^*}\right)^4 (D^* - 1)^3 \left[1 + \left(\frac{\dot{a}}{c_{\mathrm{L}}}\right)^2\right], \tag{B.6}$$

an effective beam cross-sectional area A is defined through

$$\rho A \dot{a}^2 = \mu R h \left[\frac{\pi}{24}\left(\frac{h}{R}\right)^2 + C_2 \left(\frac{\dot{a}}{c_{\mathrm{S}}}\right)^2\right] \tag{B.7}$$

and an effective dynamic foundation modulus is defined through

$$M = \frac{1}{3\pi} \frac{E_{\mathrm{d}}}{(D^* - 1)^3}. \tag{B.8}$$

Similarly, equating external work in Eq. (13) and Eq. (B.5) defines the effective pressurised width

$$W = \frac{1}{2} D \left(\frac{D^* - 2}{D^*}\right) \tag{B.9}$$

Finally, by defining a dimensionless outflow length in 'mean diameters':

$$\lambda \equiv \frac{L}{D - h} = \frac{L}{D} \frac{D^*}{D^* - 1}, \tag{B.10}$$

and a dimensionless virtual displacement $v^* \equiv v/v_0$ where

$$v_0 = \frac{4}{C_1} \frac{(D^* - 1)(D^* - 2)}{D^*} \lambda^4 \frac{p_1}{E_{\mathrm{d}}} D, \tag{B.11}$$

the profile governing equation reduces to standard form:

$$\frac{\mathrm{d}^4 v^*}{\mathrm{d}\zeta^4} + \alpha^2 \frac{\mathrm{d}^2 v^*}{\mathrm{d}\zeta^2} + m v^* = f(\zeta) \tag{B.12}$$

where $\zeta \equiv z/L$ and we have defined a geometry-sensitive dimensionless crack velocity

$$\alpha \equiv \frac{\dot{a}}{C_{\mathrm{L}}} L \sqrt{\frac{A}{I}} = \lambda \left[\frac{C_3 \left(\frac{\dot{a}}{c_{\mathrm{L}}}\right)^2 + C_4 \frac{\mu}{E} \frac{1}{(D^* - 1)^2}}{1 + \left(\frac{\dot{a}}{c_{\mathrm{L}}}\right)^2}\right]^{1/2}, \tag{B.13}$$

a dimensionless flaring modulus

$$m \equiv \frac{M L^4}{E_{\mathrm{d}} I} = \frac{8}{3\pi C_1} \frac{\lambda^4}{(D^* - 1)^2} \frac{1}{\left[1 + (\dot{a}/c_{\mathrm{L}})^2\right]}, \tag{B.14}$$

and a dimensionless pressure distribution $f(\zeta)$ within $0 < \zeta < 1$, with $f(0) = 1$ and $f(\zeta > 1) = 0$.

References

[1] B. N. Leis, X.-K. Zhu, T. Forte, E. B. Clark, Modelling running fracture in pipelines — past, present and plausible future directions, in: Proc. 11th Int. Conf. Fracture, ISBN 978-88-903188-1-8, 2005, p. Paper 5757.

[2] R. Shannon, A. Wells, Brittle crack propagation in gas filled pipelines — a model study using thin walled unplasticised PVC pipe, International Journal of Fracture 10 (4) (1974) 471–486.

[3] J. Greig, L. Ewing, Fracture propagation in polyethylene (PE) gas pipes, in: Proc. 5th International Conference on Plastic Pipes, Institute of Materials, York, 1982, pp. 13.1–13.11.

[4] G. R. Irwin, H. T. Corten, Evaluating the feasibility of basing pipeline operating pressure on in-place hydrostatic test pressure, Tech. rep., Northern Natural Gas Co. and El Paso Natural Gas Co. (1968).

[5] M. Kanninen, S. Sampath, C. Popelar, Steady-state crack propagation in pressurised pipelines without backfill, Transactions of the ASME: Journal of Pressure Vessel Technology 98 (1976) 56–64.

[6] C. Popelar, A. Rosenfeld, M. Kanninen, Steady-state crack propagation in pressurised pipelines, Transactions of the ASME: Journal of Pressure Vessel Technology 99 (1977) 112–121.

[7] P. O'Donoghue, S. T. Green, M. F. Kanninen, P. K. Bowles, The development of a fluid/structure interaction model for flawed fluid containment boundaries with applications to gas transmission and distribution piping, Computers and Structures 38 (5-6) (1991) 501–513.

[8] N. Dioh, High strain rate behaviour of polymers at various temperatures, Ph.D. thesis, University of London (1993).

[9] N. N. Dioh, J. G. Williams, P. S. Leevers, The high strain rate behaviour of polymers, Journal de Physique IV 4 (Colloque C8, supplement to Journal de Physique III) (1994) C8/119–124.

[10] P. S. Leevers, Impact and dynamic fracture of tough polymers by thermal decohesion in a Dugdale zone, International Journal of Fracture 73 (2) (1995) 109–127.

[11] M. F. Kanninen, P. E. O'Donoghue, Research challenges arising from current and potential applications of dynamic fracture mechanics to the integrity of engineering structures, International Journal of Solids and Structures 32 (17-18) (1995) 2423–2445.

[12] P. Yayla, P. S. Leevers, A new small-scale pipe test for rapid crack propagation, in: L. Ingels (Ed.), Proc. 11th Plastic Fuel Gas Pipe Symposium, American Gas Association, Arlington VA, USA, 1989, pp. 344–353.

[13] M. Wolters, G. Ketel, Some experiences with the Modified Robertson test used for study of rapid crack propagation in PE pipelines, in: Proc. 8th Plastic Fuel Gas Pipe Symposium, American Gas Association, 1983, pp. 141–146.

[14] W. Maxey, J. Kiefner, R. Eiber, A. Duffy, Ductile fracture initiation, propagation and arrest in cylindrical vessels, in: ASTM STP 514, Fracture Toughness, Proc. 1971 National Symposium on Fracture Mechanics, Part II, American Society for Testing and Materials, 1972, pp. 70–81.

[15] G. P. Venizelos, C. J. Greenshields, A. Ivankovic, P. S. Leevers, Fast brittle fracture of plastic pipes part 2:— Gas pressurised, Plastics, Rubber and Composites Processing and Applications 26 (9) (1997) 394–403.

[16] J. M. Greig, P. S. Leevers, P. Yayla, Rapid crack propagation in pressurised plastic pipe. I: Full scale and small scale RCP testing, Engineering Fracture Mechanics 42 (4) (1992) 663–673.

[17] P. Yayla, P. S. Leevers, Rapid crack propagation in pressurised plastic pipe. II: Critical pressures for polyethylene pipe, Engineering Fracture Mechanics 42 (4) (1992) 675–682.

[18] P. Vanspeybroeck, RCP, after 25 years of debates, finally mastered by two ISO tests, in: Proceedings of Plastics Pipes XI, Munich, 2001, p. 687.

[19] J. Mason, J. Chen, Establishing the correlation between S4 and full scale rapid crack propagation testing for polyamide-11 (PA-11) pipe, in: Plastics Pipes XIII, Washington DC, USA, 2006.

[20] M. Kanninen, P. E. O'Donoghue, C. Leung, S. Grigory, H. R. Couque, C. Popelar, A fracture mechanics methodology for preventing rapid crack propagation in polyethylene gas distribution pipes, in: Proc. 17th Plastic Fuel Gas Pipe Symposium, American Gas Association, San Francisco, California, USA, 1995, pp. 70 – 76.

[21] S. Grigory, M. Mamoun, A case for the use of full scale tests for effective design to prevent rapid crack propagation on PE gas pipes, in: International Plastic Pipe Symposium, 1997, pp. 147–156.

[22] Z. Zhuang, P. E. O'Donoghue, Analysis model to simulate the cracked pipe buried in soil, Acta Mechanica Sinica 14 (2) (1998) 147–156.

[23] C. J. Greenshields, P. S. Leevers, Correlation between full scale and S4 tests for Rapid Crack Propagation in plastic gas pipe, Plastics, Rubber and Composites Processing and Applications 28 (1999) 20–25.

[24] D. Edwards, D. Duval, Failure analysis of a large diameter heat-fusible pvc pipe in a horizontal directional drilling installation, in: Proc. ANTEC, Annual Technical Conference of the Society of Plastics Engineers, Vol. Annual Technical Conference, Society of Plastics Engineers, 2008.

[25] C. J. Greenshields, P. S. Leevers, The effect of air pockets on rapid crack propagation in PVC and polyethylene water pipe, Plastics Rubber and Composites Processing and Applications 24 (1995) 7–12.

[26] C. J. Greenshields, P. Davis, P. S. Leevers, Fast brittle fracture of plastic pipes part 3:— Materials and processing, Plastics, Rubber and Composites Processing and Applications 26 (9) (1997) 404–411.

[27] M. Lamborn, A. Sukhadia, Factors affecting the rapid crack propagation performance of polyethylene pipes, in: Proc. ANTEC, Annual Technical Conference of the Society of Plastics Engineers, Society of Plastics Engineers, Society of Plastics Engineers, 2010.

[28] P. O'Donoghue, M. Kanninen, G. Demofonti, S. Venzi, The development and validation of a dynamic fracture propagation model for gas transmission pipelines, International Journal of Pressure Vessels and Piping 70 (1997) 11–25.

[29] Z. Zhuang, The development of Finite Element methods for the investigation of dynamic crack propagation in gas pipelines, Ph.D. thesis, University College Dublin, Ireland (1995).

[30] Z. Zhuang, P. E. O'Donoghue, The recent development of analysis methodology for rapid crack propagation and arrest in gas pipelines, International Journal of Fracture 101 (1999) 269–290.

[31] Z. Zhuang, P. E. O'Donoghue, Determination of material fracture toughness by a computational/experimental approach for rapid crack propagation in PE pipe, International Journal of Fracture 101 (3) (2000) 251–268.

[32] A. Ivankovic, G. P. Venizelos, Rapid Crack Propagation in plastic pipe: predicting full-scale critical pressure from S4 test results, Engineering Fracture Mechanics 59 (5) (1998) 607–622.

[33] C. J. Greenshields, G. P. Venizelos, A. Ivankovic, A fluid-structure model for fast brittle fracture in plastic pipes, Journal of Fluids and Structures 14 (2000) 221–234.

[34] S. Nilsson, K. Thörnblom, S.-E. Sällberg, G. Bergström, Brittle fracture in casing pipes, in: Proc. 10th International Symposium on District Heating and Cooling, Hanover, Germany, 2006.

[35] C. J. Greenshields, P. S. Leevers, Rapid crack propagation in plastic water pipes: measurement of dynamic fracture resistance, International Journal of Fracture 79 (1996) 85–95.

[36] J. G. Williams, G. P. Venizelos, A perturbation analysis of Rapid Crack Propagation in pressurised pipe, International Journal of Fracture 94 (2) (1998) 161–176.

[37] M. F. Kanninen, An augmented double cantilever beam model for studying crack propagation and arrest, International Journal of Fracture 9 (1) (1973) 83–92.

[38] G. Alder, I. Christie, J. Roberts, Energy balance models for ductile fracture propagation in gas pipelines, Tech. rep., Department of Civil Engineering and Building Science, Department of Mechanical Engineering, University of Edinburgh (1984).

[39] A. L. Addy, B. J. Walker, Rapid discharging of a vessel through a nozzle or orifice, ASME 72-FE-40.

[40] J. Owczarek, Fundamentals of Gas Dynamics, International Textbook Company, 1964.

[41] R. J. Roark, Roark's formulas for stress and strain, 6th Edition, McGraw-Hill, Inc., 1975.

[42] M. F. Kanninen, Research in progress on unstable crack propagation in pressure vessels and pipelines, International Journal of Fracture 6 (1) (1970) 94–96.

[43] C. J. Greenshields, P. S. Leevers, The effect of pressurising fluid on fast fracture in plastic water pipes, in: Plastics Pipes IX, Proc. 9th Int. Conf. Plastics Pipes, IOM Communications, London, Edinburgh, 1995.

[44] A. Ivankovic, V. Tropsa, H. Jasak, P. S. Leevers, Fully predictive model of RCP in plastic pipes, in: Proc. 14th European Conf. Fracture, EMAS Publications, Krakow, Poland, 2002.

[45] P. S. Leevers, Crack front shape effects in the Double Torsion test, Journal of Materials Science 17 (1982) 2469–2480.

References

[1] B. N. Leis, X.-K. Zhu, T. Forte, E. B. Clark, Modelling running fracture in pipelines — past, present and plausible future directions, in: Proc. 11th Int. Conf. Fracture, ISBN 978-88-903188-1-8, 2005, p. Paper 5757.

[2] R. Shannon, A. Wells, Brittle crack propagation in gas filled pipelines — a model study using thin walled unplasticised PVC pipe, International Journal of Fracture 10 (4) (1974) 471–486.

[3] J. Greig, L. Ewing, Fracture propagation in polyethylene (PE) gas pipes, in: Proc. 5th International Conference on Plastic Pipes, Institute of Materials, York, 1982, pp. 13.1–13.11.

[4] G. R. Irwin, H. T. Corten, Evaluating the feasibility of basing pipeline operating pressure on in-place hydrostatic test pressure, Tech. rep., Northern Natural Gas Co. and El Paso Natural Gas Co. (1968).

[5] M. Kanninen, S. Sampath, C. Popelar, Steady-state crack propagation in pressurised pipelines without backfill, Transactions of the ASME: Journal of Pressure Vessel Technology 98 (1976) 56–64.

[6] C. Popelar, A. Rosenfeld, M. Kanninen, Steady-state crack propagation in pressurised pipelines, Transactions of the ASME: Journal of Pressure Vessel Technology 99 (1977) 112–121.

[7] P. O'Donoghue, S. T. Green, M. F. Kanninen, P. K. Bowles, The development of a fluid/structure interaction model for flawed fluid containment boundaries with applications to gas transmission and distribution piping, Computers and Structures 38 (5-6) (1991) 501–513.

[8] N. Dioh, High strain rate behaviour of polymers at various temperatures, Ph.D. thesis, University of London (1993).

[9] N. N. Dioh, J. G. Williams, P. S. Leevers, The high strain rate behaviour of polymers, Journal de Physique IV 4 (Colloque C8, supplement to Journal de Physique III) (1994) C8/119–124.

[10] P. S. Leevers, Impact and dynamic fracture of tough polymers by thermal decohesion in a Dugdale zone, International Journal of Fracture 73 (2) (1995) 109–127.

[11] M. F. Kanninen, P. E. O'Donoghue, Research challenges arising from current and potential applications of dynamic fracture mechanics to the integrity of engineering structures, International Journal of Solids and Structures 32 (17-18) (1995) 2423–2445.

[12] P. Yayla, P. S. Leevers, A new small-scale pipe test for rapid crack propagation, in: L. Ingels (Ed.), Proc. 11th Plastic Fuel Gas Pipe Symposium, American Gas Association, Arlington VA, USA, 1989, pp. 344–353.

[13] M. Wolters, G. Ketel, Some experiences with the Modified Robertson test used for study of rapid crack propagation in PE pipelines, in: Proc. 8th Plastic Fuel Gas Pipe Symposium, American Gas Association, 1983, pp. 141–146.

[14] W. Maxey, J. Kiefner, R. Eiber, A. Duffy, Ductile fracture initiation, propagation and arrest in cylindrical vessels, in: ASTM STP 514, Fracture Toughness, Proc. 1971 National Symposium on Fracture Mechanics, Part II, American Society for Testing and Materials, 1972, pp. 70–81.

[15] G. P. Venizelos, C. J. Greenshields, A. Ivankovic, P. S. Leevers, Fast brittle fracture of plastic pipes part 2:— Gas pressurised, Plastics, Rubber and Composites Processing and Applications 26 (9) (1997) 394–403.

[16] J. M. Greig, P. S. Leevers, P. Yayla, Rapid crack propagation in pressurised plastic pipe. I: Full scale and small scale RCP testing, Engineering Fracture Mechanics 42 (4) (1992) 663–673.

[17] P. Yayla, P. S. Leevers, Rapid crack propagation in pressurised plastic pipe. II: Critical pressures for polyethylene pipe, Engineering Fracture Mechanics 42 (4) (1992) 675–682.

[18] P. Vanspeybroeck, RCP, after 25 years of debates, finally mastered by two ISO tests, in: Proceedings of Plastics Pipes XI, Munich, 2001, p. 687.

[19] J. Mason, J. Chen, Establishing the correlation between S4 and full scale rapid crack propagation testing for polyamide-11 (PA-11) pipe, in: Plastics Pipes XIII, Washington DC, USA, 2006.

[20] M. Kanninen, P. E. O'Donoghue, C. Leung, S. Grigory, H. R. Couque, C. Popelar, A fracture mechanics methodology for preventing rapid crack propagation in polyethylene gas distribution pipes, in: Proc. 17th Plastic Fuel Gas Pipe Symposium, American Gas Association, San Francisco, California, USA, 1995, pp. 70 – 76.

[21] S. Grigory, M. Mamoun, A case for the use of full scale tests for effective design to prevent rapid crack propagation on PE gas pipes, in: International Plastic Pipe Symposium, 1997, pp. 147–156.

[22] Z. Zhuang, P. E. O'Donoghue, Analysis model to simulate the cracked pipe buried in soil, Acta Mechanica Sinica 14 (2) (1998) 147–156.

[23] C. J. Greenshields, P. S. Leevers, Correlation between full scale and S4 tests for Rapid Crack Propagation in plastic gas pipe, Plastics, Rubber and Composites Processing and Applications 28 (1999) 20–25.

[24] D. Edwards, D. Duval, Failure analysis of a large diameter heat-fusible pvc pipe in a horizontal directional drilling installation, in: Proc. ANTEC, Annual Technical Conference of the Society of Plastics Engineers, Vol. Annual Technical Conference, Society of Plastics Engineers, 2008.

[25] C. J. Greenshields, P. S. Leevers, The effect of air pockets on rapid crack propagation in PVC and polyethylene water pipe, Plastics Rubber and Composites Processing and Applications 24 (1995) 7–12.

[26] C. J. Greenshields, P. Davis, P. S. Leevers, Fast brittle fracture of plastic pipes part 3:— Materials and processing, Plastics, Rubber and Composites Processing and Applications 26 (9) (1997) 404–411.

[27] M. Lamborn, A. Sukhadia, Factors affecting the rapid crack propagation performance of polyethylene pipes, in: Proc. ANTEC, Annual Technical Conference of the Society of Plastics Engineers, Society of Plastics Engineers, Society of Plastics Engineers, 2010.

[28] P. O'Donoghue, M. Kanninen, G. Demofonti, S. Venzi, The development and validation of a dynamic fracture propagation model for gas transmission pipelines, International Journal of Pressure Vessels and Piping 70 (1997) 11–25.

[29] Z. Zhuang, The development of Finite Element methods for the investigation of dynamic crack propagation in gas pipelines, Ph.D. thesis, University College Dublin, Ireland (1995).

[30] Z. Zhuang, P. E. O'Donoghue, The recent development of analysis methodology for rapid crack propagation and arrest in gas pipelines, International Journal of Fracture 101 (1999) 269–290.

[31] Z. Zhuang, P. E. O'Donoghue, Determination of material fracture toughness by a computational/experimental approach for rapid crack propagation in PE pipe, International Journal of Fracture 101 (3) (2000) 251–268.

[32] A. Ivankovic, G. P. Venizelos, Rapid Crack Propagation in plastic pipe: predicting full-scale critical pressure from S4 test results, Engineering Fracture Mechanics 59 (5) (1998) 607–622.

[33] C. J. Greenshields, G. P. Venizelos, A. Ivankovic, A fluid-structure model for fast brittle fracture in plastic pipes, Journal of Fluids and Structures 14 (2000) 221–234.

[34] S. Nilsson, K. Thörnblom, S.-E. Sällberg, G. Bergström, Brittle fracture in casing pipes, in: Proc. 10th International Symposium on District Heating and Cooling, Hanover, Germany, 2006.

[35] C. J. Greenshields, P. S. Leevers, Rapid crack propagation in plastic water pipes: measurement of dynamic fracture resistance, International Journal of Fracture 79 (1996) 85–95.

[36] J. G. Williams, G. P. Venizelos, A perturbation analysis of Rapid Crack Propagation in pressurised pipe, International Journal of Fracture 94 (2) (1998) 161–176.

[37] M. F. Kanninen, An augmented double cantilever beam model for studying crack propagation and arrest, International Journal of Fracture 9 (1) (1973) 83–92.

[38] G. Alder, I. Christie, J. Roberts, Energy balance models for ductile fracture propagation in gas pipelines, Tech. rep., Department of Civil Engineering and Building Science, Department of Mechanical Engineering, University of Edinburgh (1984).

[39] A. L. Addy, B. J. Walker, Rapid discharging of a vessel through a nozzle or orifice, ASME 72-FE-40.

[40] J. Owczarek, Fundamentals of Gas Dynamics, International Textbook Company, 1964.

[41] R. J. Roark, Roark's formulas for stress and strain, 6th Edition, McGraw-Hill, Inc., 1975.

[42] M. F. Kanninen, Research in progress on unstable crack propagation in pressure vessels and pipelines, International Journal of Fracture 6 (1) (1970) 94–96.

[43] C. J. Greenshields, P. S. Leevers, The effect of pressurising fluid on fast fracture in plastic water pipes, in: Plastics Pipes IX, Proc. 9th Int. Conf. Plastics Pipes, IOM Communications, London, Edinburgh, 1995.

[44] A. Ivankovic, V. Tropsa, H. Jasak, P. S. Leevers, Fully predictive model of RCP in plastic pipes, in: Proc. 14th European Conf. Fracture, EMAS Publications, Krakow, Poland, 2002.

[45] P. S. Leevers, Crack front shape effects in the Double Torsion test, Journal of Materials Science 17 (1982) 2469–2480.